Ground ozone rise caused by the larger emission reduction of nitrogen oxides than volatile organic components

Qian Wang[a,b], Yuewu Li [b], Fangqian Zhong[c], Jianbin Wu[c,d], Wanqi Wu[a], Hongliang Zhang[a], Rong Wang[a], Yusen Duan [b], Qingyan Fu[b,1], Qing Li[a], Lin Wang[a], Shaocai Yu[e], Abdewahid Mellouki[g], Jianmin Chen[a,f,1]

[a] Shanghai Key Laboratory of Atmospheric Particle Pollution and Prevention (LAP[3]), Department of Environmental Science & Engineering, Institute of Atmospheric Sciences, Fudan University, Shanghai 200438, China;

[b] Shanghai Environmental Monitoring Center, Shanghai 200235, China;

[c] 3Clear Technology Co.,Ltd.,Beijing 100029,China;

[d] Institute of Atmospheric Physics, Chinese Academy of Sciences, Beijing 100029, China;

[e] College of Environmental and Resource Sciences, Zhejiang University, Hangzhou 310058, China;

[f] Institute of Eco-Chongming (IEC), 3663 N. Zhongshan Rd., Shanghai 200062, China;

[g] Institut de Combustion, Aérothermique, Réactivité et Environnement, CNRS, 45071 Orléans CEDEX 02, France.

Author Contributions: Q.W., H.Z., R.W., Y.D., Q.F., Q.L., L.W., S.Y., A.M. and J.C. designed research; Q.W., Y.L., F.Z., and J.W. performed research; Q.W., Y.L., F.Z., J.W., and W.W. analyzed data; and Q.W., Y.L., W.W., and J.C. wrote the paper.

The authors declare no conflict of interest.

This article is a PNAS Direct Submission.

[1] To whom correspondence may be addressed. **Email:** jmchen@fudan.edu.cn or qingyanf@sheemc.cn

Keywords: O_3 rise, the 2022 lockdown, VOCs, emission control scenarios

Abstract

Ground-level ozone (O_3) pollution has shifted from being a scientific topic to a governmental imperative in China. We analyze the mechanism for the O_3 rise observed in Shanghai during the lockdown in the spread of COVID-19 in 2022 by combining utilizing ground-level observed data, an observation-based model, and a chemical transport model. We find that the increase in O_3 can be mainly attributable to the larger emission reduction of nitrogen oxides (NOx) than volatile organic components (VOCs), of which the effect is amplified by the adverse meteorological conditions. The chemical transport modeling results suggest that a higher ratio of emission reduction of NOx to VOCs increases the daily maximum 8-hour moving average O_3 concentration considerably relative to a counterfactual scenario assuming the same ratio of emission reduction of NOx to VOCs. This indicates that the concentration of O_3 would depends not only on the strength of emission reduction but also the ratio of emission reduction between species. Our results highlight the importance of well-designed strategies with appropriate control of the VOCs to NOx ratio to mitigate O_3 pollution in cities.

Significance Statement

O_3 pollution has become increasingly prominent in many cities of China. Governmental mandatory lockdown measures in many megacities led to unprecedented reductions in primary emissions, improvements in ambient air quality but increases in O_3. This study finds that the increasing O_3 in Shanghai during the lockdown in the spread of COVID-19 in 2022 resulted from ineffective VOCs to NOx emission reduction ratio and adverse meteorological conditions. Emission reduction policies for VOCs are most effective for decreasing O_3. Only well-designed control strategies with reasonable control ratios for VOCs and NOx emissions should be promoted to mitigate O_3 pollution.

Introduction

Ground-level ozone (O_3) is a secondary air pollutant formed nonlinearly by photochemical reactions of volatile organic compounds and nitrogen oxides(1-5), which is associated with climate, ecosystems, and human health(6-10).

O_3 pollution in China has been the subject of widespread concern (11-14). Surface O_3 levels did not show any declining trend while $PM_{2.5}$ concentrations of 74 major cities across China decreased by 58% from 2013 to 2022. Particularly since COVID-19, many cities have implemented mandatory lockdown measures to curb the transmission of coronavirus disease during the corresponding lockdown periods (CLPs), O_3 has really shifted from being a scientific topic to a governmental imperative in China. Therefore, CLPs provide a unique opportunity to reshape our understanding of how O_3 respond to sharp reductions in air pollutant emissions and how to effectively alleviate O_3 pollution.

Air quality changes including O_3 were analyzed in various cities around the world during CLPs, using ground-based observations and satellite measurements, as well as model simulation (15-24). Anthropogenic NOx emissions dropped by at least 15% globally according to the report from a multi-constituent chemical data assimilation system, while free tropospheric ozone increased by up to 5 ppt, consistent with independent satellite observations (20). The decrease of NO_2 is in general agreement with emission inventories that account for lockdown periods. However, O_3 increased during mandatory lockdown measures (19, 22, 25-27). Satellite images of the massive reduction in NO_2 was directly observed by National Aeronautics and Space Administration (NASA) over China resulting from the economic slow-down and reduction in human activities (NASA, 2020). O_3 increased in urban areas during the same COVID period that NOx and VOCs emissions sharply reduced (23, 27-32). Sudden decreases in deweathered NO_2 concentrations and increases in O_3 in 11 cities globally were demonstrated via a deweathering machine learning technique(33). The total gaseous oxidant ($Ox = NO_2 + O_3$) showed limited change. Recent studies suggest that weakened nitration, increased photochemical formation, and decreased $PM_{2.5}$ contributed to the increase in O_3 during the pandemic lockdown(19, 23, 33-35). Synergistic observation analyses and model simulations in China showed that nitrogen oxide reductions resulted in ozone increases in urban areas due to nonlinear chemistry production and titration of ozone by NO. These conditions further increased the atmospheric oxidizing capacity and facilitated secondary aerosol formation under adverse meteorological conditions during the COVID-19 outbreak in China (24). The NOx reductions counteracted the O_3 decreases and increased nighttime NO_3 radical formation, which increased atmospheric oxidizing capacity and facilitated the formation of secondary inorganic and organic particulate matter (34). Furthermore, accelerated $OH-HO_2-RO_2$ radical cycling may have played a role (36). The increase in O_3 may have been due to lower fine particle loadings, which led to less scavenging of HO_2 and greater O3 production (23).

Shanghai is one of the most developed megacities, which is known as a financial, commercial and transport center in China. From April to May 2022(hereafter referred to as CLP-22)., Shanghai imposed the extremely stringent measures to eliminate the COVID's spread. These measures severely limited human activities and manufacturing production, resulting in rapid and massive emission reductions. However, O_3 concentration during CLP-22 increased significantly. Comparing with the previous CLPs, CLP-22 occurred in high O_3 pollution season, which is more indicative to understanding O_3 pollution to sharp reduction of emissions. The previous study indicated the high O_3 concentrations in 2022 of Shanghai were mainly due to large reductions in the emissions of NOx and that the decrease in the concentrations of volatile organic compounds (VOCs) could not overcome the NO titration effect(37). However, how the response of O_3 to its precursors and VOCs/ NOx impacts at urban scale during the COVID lockdown period was rarely identified.

In this study, we detailed the possible formation pathway of O_3 in April and May, 2022 in Shanghai, by using surface observation and observation-based model. The meteorological and emission effects on O_3 levels were identified based on chemical transport model simulations. The response of O_3 to different VOCs/NOx control scenarios was also simulated, to evaluate the efficiency of emission control strategies and guide future emission control policies to alleviate ozone pollution.

Results

Significant O_3 increases in megacities during COVID-19 lockdown periods. NO_2 concentration was reduced significantly in all countries during the lockdown, except Australia and Denmark as illustrated in Figure S1. The reduction ranged from 10% to 151%. However, 75.9% of the countries showed an increasing trend of O_3 concentration, averaging 17%(38).

Megacities in China, such as Wuhan (WH), Xi 'an (XA), Jilin (JL), Shenzhen (SZ), Shanghai (SH) and Beijing (BJ) were severely impacted by COVID and took strict control measures to eliminate its spread(21, 24, 39-42). Concentration changes of typical air pollutants during the resulting lockdown periods were significantly reduced when compared with the mean measurements of the last three years, as shown in Figure 1. The largest decreases in NO_2 were found in Wuhan and Shanghai with the reduction of 57.1% and 54.5%, respectively. $PM_{2.5}$ and PM_{10} also showed over 35% reduction. However, an increase in O_3 between 3 and 53% was found in all megacities in China, including Wuhan (WH), Xi 'an (XA), Jilin (JL), Shenzhen (SZ), Shanghai (SH) and Beijing (BJ). Reductions in $PM_{2.5}$, PM_{10}, and NO_2 concentrations, as well as increases in O_3 concentration, were closely related to the population density and the length of CLPs.

The diurnal variation exhibited a similar pattern for both NO_2 and O_3 among those six cities during CLPs across all cities(43),as shown in Fig. 2C. The significant decrease in NO_2 occurred throughout the day in these cities, especially during morning and evening rush hours. The increase in O_3 during night-time was observed to be higher than day-time. This was mainly because of night-time reductions in nitrogen oxides, which could form nitric acid, oxidize hydrocarbons, and remove O_3 (44-46).

O_3 and precursor level changes in Shanghai. Three monitoring sites were selected, namely Pudong Site (Pudong), Jinshan Xincheng Site (Jinshan), and Qingpu Dianshanhu Site (Qingpu) representing urban agglomeration, petrochemical engineering, and a suburb of the Jiangsu and Zhejiang provinces, respectively. Diurnal variations of NO_2, VOCs, and O_3 during CLP-22 in the three sites were obtained, as well as last year’s data.

The concentrations of NO_2 and VOCs in Pudong during CLP-22 showed the largest decreases of 46.7% and 50% when compared with the same period in 2021, especially during the morning and evening rush hours (Fig. 2). Economic and social activities in Shanghai were stringently limited during CLP-22, leading to noticeable decreases in emission sources of air pollutants in urban areas such as Pudong. The levels of NO_2 and VOCs in Jinshan, an industrial area, had the smallest decreases of 22.7% and 30.8%, respectively. O_3 concentrations in these stations showed substantial increases, with the largest of 27.1% in Pudong, 25.6% in Qingpu, and the smallest of 12.6% in Jinshan. Generally, the difference between peak and valley values in diurnal ozone concentration reflect the ozone formation potentials during daytime. Fig.2 shows that the diurnal increase in Pudong was the smallest, at 62.7%, but due to the rise in the background concentration at night, the mean O_3 during CLP-22 increased by 27.1% compared to the same period of last year, which was the greatest among the three stations. Qingpu has the strongest O_3 formation capacity, with a day-night change of 123% leading to the high increase of 25.6% in O_3, which was greater than that of 12.6% in Jinshan.

Compared to last year, the largest decrease of alkanes, alkenes, aromatic hydrocarbons and alkynes during CLP-22 was identified in Pudong, with reductions of 47.2%, 48.8%, 63.8%, and 72.2%, respectively. The smallest decrease of alkene was observed in Qingpu, with a 13.4% reduction. Similarly, VOCs concentrations in three sites during CLP-22 were analyzed and compared with the same period last year, as shown in Figure S3. It shows that the concentration of alkanes in Pudong, Jinshan and Qingpu during CLP-22 accounted for 71.8%, 56.4% and 55.6%, respectively, which is the dominant group in VOCs concentration; followed by alkenes, which accounted for 12.1%, 21.6% and 20.8%, respectively; and then aromatic hydrocarbons and alkynes. Compared with the same period in 2021. It can be seen that alkenes contribution in Pudong and Qingpu increased, while slightly decreasing in Jinshan.

The concentrations of the top 20 VOC components during CLP-22 are compared with the same period of last year in Figure S3. The top 20 components in Pudong accounted for 93% of the total concentration of VOCs. Compared with the same period last year, the concentrations of all of these components decreased, in particular ethane, propane and ethylene. In Jinshan, the top 20 components accounted for 99% of the total, with ethane, methane and propylene having the highest concentrations. In comparison to last year, the majority of these components decreased, though several increased—including ethane, 1,2, 4-trimethylbenzene, and 1, 3-butadiene. In Qingpu, the top 20 components accounted for 92% of the total, with propane, ethane and ethylene having the highest concentrations. There were many other components that had higher measurements than last year, such as benzene, 1-Henenxe, 2, 3, 4-trimethypentane, trans – 2-butene, isopropylbenzene, methylcyclohexane, and 2 – methylheptane.

Cause analysis of O_3 changes. We adopted the ozone formation potentials (OFP), which is the product of the mixing ratio of VOC compounds and the maximum incremental reactivity (MIR), developed by Carter, to evaluate the impact of VOC species on ozone formation (47).

Comparing the OFP of VOC components during CLP-22 to the previous year, OFP of alkenes in Pudong accounted for 36.6%, which was significantly higher than the 28.6% measured last year, joining aromatics as the dominant categories for ozone formation (Figure S4). Among the alkenes, ethylene, propylene, toluene, m-p-xylene and o-xylene accounted for the highest proportion, with the total contribution at about 58.8%. OFP of alkenes in Qingpu had the largest increase (63.3%), up from 30% last year. Trans-2-butene and 1-hexene were both up from last year and, together with ethylene, propylene and isoprene, became the top five contributors—accounting for 58.7% in total. This indicates these specific alkenes may have been contributed more O_3 formation in Qingpu during CLP-22(48, 49). The OFP contribution ratio of various VOCs in Jinshan is similar to the ratio measured last year: mainly alkenes, then aromatic hydrocarbon and alkanes. The OFP contribution of propylene, cis-2-butene, ethylbenzene, 1, 2, 4-trimethylbenzene and o-xylene were the highest, accounting for 74.2% in total.

Based on the observation data from those three sites, an observation-based model (OBM) was used to analyze ozone formation mechanism during CLP-22 (Fig. 3A). It was found that O_3 concentration is substantially limited by VOCs in all three stations. Compared to the same period last year, OFP has decreased in Pudong, and increased in Qingpu. OFP in Jinshan remained pretty much the same. This is also consistent with the measured changes of VOCs at all three stations. The OFP contribution of various VOC components in Qingpu has risen under the influence of regional emissions and meteorological conditions(Fig. 3B). This led to the large increase in ozone observed there. The OFP in Pudong has weakened, however, due to significant reductions in NOx emissions, the night-time weakening of the titration effect, and the background concentration of ozone. Ozone measurements in Pudong still ended up high in value. The OFP in Jinshan and the nighttime background concentration of O_3 did not change much, resulting in a relatively small increase in O_3.

Scenarios of NOx and VOC reduction to elucidate O_3 rise. In order to investigate how O_3 responses to NOx and VOCs emissions change, one baseline and 18 sets of emission control scenarios have been designed to simulate CLP-22 by using a regional chemical transport model (Fig. S5). In the sensitivity scenarios, different VOCs and NOx reduction ratios were designed to quantify the response of O_3 concentrations in three sites during CLP-22.

Fig. 4 shows hourly average, maximum daily and MDA8 (the maximum daily 8-h moving average) O_3 concentrations under various emission control scenarios relative to the base scenario during CLP-22. Different emission reduction rates may lead to different control effects on O_3 (50). According to the changes in observed NO_2 and VOCs concentrations, the real emission reduction percentages of the three sites were predicted as shown in Fig. 4. O_3 hourly average concentration showed decreasing trends in all three sites only under the VOCs-only emission reduction scenarios. The increasing trends under the predicted reduction percentages were consistent with the observed trends among the three sites, with the highest in Pudong and smallest in Jinshan. This is mainly because the decrease in NOx emissions could affect the removal of O_3 at night. However, the maximum daily and MDA8 O_3 concentrations showed different trends. With the VOCs-only emission control scheme, larger emission reduction percentages led to a significant reduction in daily maximum and MDA8 O_3 concentrations, by nearly 10 $\mu g/m^3$ in Pudong. Under the aromatics-only, alkenes-only, or VOCs-only emission control scenarios with a reduction percentage of 100%, daily maximum and MDA8 O_3 concentrations showed the same decreasing effects with a ratio of 2 to 1 for VOCs and NOx emission control scenarios. This means that controlling specific, active VOCs emissions could be effective in reducing O_3, especially its alkene and aromatic components. It's worth noting that with scenarios like NOx-only emission reductions or with a greater NOx reduction than VOCs, MAD8 O_3 concentration showed an increasing trend when the total reduction percentage was not too large, especially in Pudong. That explains why the high O_3 increasing trend was found in Pudong. In regions such as Pudong with elevated NOx concentrations due to high emissions density, reductions in NOx will lead to an increase in local ozone concentrations. This echoed the VOCs limited conditions for the O_3 formation in Yangtze River

Delta and many other urban areas(51-53). O_3 concentration in Jinshan also showed this trend, but the variation was smaller than in Pudong. This might be because Jinshan was dominated by a southeastern wind during CLP-22; Jinshan is in the southern region of Shanghai, with high VOCs emission densities. Qingpu is a rural region, located west of Shanghai, and was easily influenced by regional transport of pollution from Jiangsu and Zhejiang. Meanwhile, the increasing trends of some alkenes in Qingpu were observed as stated earlier. Therefore, although the predicted MDA8 O_3 concentration shows slight decreasing trends under the NOx and VOCs emission reduction scenarios, the high increasing trends of MAD8 O_3 concentration were still observed in Qingpu. With the aid of a chemical transport model, we have shown that the increases in O_3 during CLP-22 in those three sites were affected by both adverse weather conditions and emission changes (Fig. 5). Adverse meteorological conditions, including high temperatures and low relative humidity, caused an increase of O_3 concentrations from2 to 7 μg/m^3 in those three sites, with the greatest increase in Pudong; while emissions changes caused a rise from 3 to 17 μg/m^3, with the greatest increase in Qingpu (Fig. 3A and 5). This indicated that the reduction in precursor emissions during CLP-22, including NOx/VOCs emission changes, and an increase in some of the active components of VOCs as well as the influence of regional transportation of emissions outside of Shanghai caused an increase in O_3 concentration, especially in Qingpu (54).

Overall, adverse meteorological conditions(55, 56), NOx/VOCs emission changes, and an increase in some active components of VOCs may have played an important role in the increase in O_3. The results demonstrate that reliable air quality improvements need more sophisticated emission control strategies rather than simple, one-fits-all control measures. In summary, the results indicated that O_3 pollution in Shanghai, particularly in urban areas, was directly affected by VOCs emissions. Hence, policymakers need to pay more attention to VOCs emission controls, especially for alkenes. Furthermore, regional joint prevention and cooperation is necessary for mitigating O_3 pollution.

Discussion

Significant decreases in primary pollutants were observed during CLPs in most cities worldwide, but there was a corresponding increase in O_3. A COVID outbreak took place in April and May, 2022 in Shanghai, the most developed metropolitan city in China. The local government adopted extremely stringent lockdown measures, which led to sharp reductions in pollutant emissions. While most air pollutants, such as NO_2, SO_2, $PM_{2.5}$, and PM_{10}, decreased significantly during CLP-22 compared to the same period of 2021, O_3 concentration levels showed an unexpected increasing trend. Comparing with the previous CLPs, CLP-22 occurred in high O_3 pollution season, which is more indicative to reshape our understanding of how O_3 responds to sharp reductions in anthropogenic emissions. Finding solutions to curb O_3 pollution remains an important issue. This study focused on the change of O_3 and its precursors in Shanghai during CLP-22; an OBM and a chemical transport model were used to explore potential influences of emissions changes and provide a scientific reference for controlling O_3 pollution in the future.

The study revealed that increasing O_3 trends in Shanghai during CLP-22 were primarily driven by ineffective VOCs and NOx reduction ratios and adverse meteorological conditions. Model results indicate that high VOCs emission reduction scenarios were most effective in decreasing MDA8 O_3 concentrations, whereas emission control scenarios with higher NOx reductions than VOCs may lead to increasing O_3, especially in urban areas. Simple, one-fits-all control measures such as short-term lockdown strategies may not achieve the control targets for both primary and secondary air pollution. The results of this study provide justification for city-level initiatives to promote effective VOCs and NOx control policies as well as regional cooperation.

Materials and Methods

In situ observations. Observational data for $PM_{2.5}$, PM_{10}, NO_2, SO_2, O_3, and CO were taken from the standard environmental monitoring network, which was established by the Ministry of Ecology and Environment. City-level data are calculated by nationally controlled sites to represent the urban-scale air quality level. This ensured that the quality of data used in this paper was authoritative and guaranteed by the government.

VOCs data. In this study, VOCs data from three stations were analyzed. Concentrations of VOC components were automatically monitored by gas chromatography-hydrogen flame ionization detectors (GC-FID) at all three sites. Monitoring equipment included PAMS components, which can generate one set of data per hour. A PE company monitor (PerkinElmer 300TD VOC) was used at Pudong station, while the cities of Jinshan and Qingpu used a Chromatotech A11000. These three sites all follow the unified operation quality control standards of the state and Shanghai. Thus, the data quality is good and data efficiency exceeds 85%.

Observation-based model. A box model based on the Carbon Bond mechanism was utilized to simulate O_3 sensitivities in this study(57). Observations of C2-C12 hydrocarbons, trace gases (NO, NO_2, O_3, and CO), and meteorological parameters served as the input for this model. Relative incremental reactivity (RIR) was calculated to assess sensitivity of O_3 formation with respect to its precursors.

Chemical transport model. The Weather Research and Forecasting (WRFv4.3.1) and Community Multiscale Air Quality Modeling (CMAQv5.3.3) with SAPRC-07 chemical mechanism and AERO7 module were utilized to simulate spatiotemporal variations of O_3 (47, 58, 59).Three domains with horizontal grid resolutions of 27, 9, and 3 km were set up. Anthropogenic emissions data from outside China came from the Emissions Database for Global Atmospheric Research (EDGAR) (60). Emissions data for the area outside the YRD region in China were derived from the Multi-resolution Emissions Inventory for China (MEIC) developed by Tsinghua University (http://www.meicmodel.org). The local emissions inventories for the YRD region and Shanghai were developed by the Shanghai Academy of Environment and Science and the Shanghai Environmental Monitoring Center, respectively(61-65). The biogenic emissions were calculated by the Model of Emissions of Gas and Aerosols from Nature (MEGAN). The correlation coefficient(R), root mean square error(RMSE) and normalized mean bias (NMB) was adopted to quantitatively evaluate the performance of both

WRF and CMAQ models used in this study. Table S1 shows the statistical evaluation of wind speed at 10m (WS_{10}), air temperature at 2m (T_2), and relative humidity at 2m (RH) of three monitoring sites in Shanghai during CLP-22. In general, the WRF performance is comparable to previous studies in the YRD region to support further air quality simulations(66). The correlation coefficient between simulated and observed hourly O_3 concentrations during CLP-22 in Pudong, Jinshan and Qingpu was 0.75, 0.72 and 0.68, respectively. Overall, the model performances is comparable to the previous modeling studies(66-70).

ACKNOWLEDGMENTS. This work was funded by the Ministry of Science and Technology of China (2022YF3701100 and 2022YFC3703504), the National Joint Center for Air Pollution Prevention and Control of China (DQGG202123), the National Natural Science Foundation of China (Nos. 91843301 and 92043301), the Science & Technology Commission of Shanghai Municipality (No.1DZ1202300 and No.20dz1204000), the Shanghai International Science and Technology Partnership Project (No. 21230780200), and the European Union's Horizon 2020 research and innovation program (MARSU, 690958). Thanks for the effort contributed by the reviewers toward improving the manuscript.

References

1. A. M. Thompson, The Oxidizing Capacity of the Earth's Atmosphere: Probable Past and Future Changes. *Science, New Series* **256**, 1157-1165 (2016).
2. P. CRUTZEN, A Discussion of the Chemistry of Some Minor Constituents in the Stratosphere and Troposphere. *Pure and Applied Geophysics (PAGEOPH)* **Vol. 106-108 (1973/V-VII)**, 1385-1399 (1973).
3. L. I. Kleinman *et al.*, Ozone production efficiency in an urban area. *Journal of Geophysical Research: Atmospheres* **107**, ACH 23-21-ACH 23-12 (2002).
4. S. Sillman, The relation between ozone, NO and hydrocarbons in urban and polluted rural environments. *Atmospheric Environment* **33**, 1821—1845 (1999).
5. R. Atkinson, Atmospheric chemistry of VOCs and NOx. *Atmospheric Environment* **34 (2000)**, 2063-2101 (1998).
6. L. S. i. b. a. M. R. A. J. Fuhrer, Critical Levels for Ozone Effects on Vegetation in Europe. *Environmental Pollution* **97**, 91-106 (1997).
7. M. J. Hollaway, S. R. Arnold, A. J. Challinor, L. D. Emberson, Intercontinental trans-boundary contributions to ozone-induced crop yield losses in the Northern Hemisphere. *Biogeosciences* **9**, 271-292 (2012).
8. A. S. Lefohn *et al.*, Responses of human health and vegetation exposure metrics to changes in ozone concentration distributions in the European Union, United States, and China. *Atmospheric Environment* **152**, 123-145 (2017).
9. X. Yue *et al.*, Ozone and haze pollution weakens net primary productivity in China. *Atmospheric Chemistry and Physics* **17**, 6073-6089 (2017).
10. E. A. Ainsworth, C. R. Yendrek, S. Sitch, W. J. Collins, L. D. Emberson, The effects of tropospheric ozone on net primary productivity and implications for climate change. *Annu Rev Plant Biol* **63**, 637-661 (2012).

11. T. J. Wang *et al.*, Integrated studies of a photochemical smog episode in Hong Kong and regional transport in the Pearl River Delta of China. *Tellus B: Chemical and Physical Meteorology* **58**, 31-40 (2017).
12. T. Wang *et al.*, Ozone pollution in China: A review of concentrations, meteorological influences, chemical precursors, and effects. *Sci Total Environ* **575**, 1582-1596 (2017).
13. X. Xu *et al.*, Long-term trend of surface ozone at a regional background station in eastern China 1991-2006: enhanced variability. *Atmospheric Chemistry and Physics* **8**, 2595-2607 (2008).
14. A. J. Ding *et al.*, Ozone and fine particle in the western Yangtze River Delta: an overview of 1 yr data at the SORPES station. *Atmospheric Chemistry and Physics* **13**, 5813-5830 (2013).
15. F. Fu, K. L. Purvis-Roberts, B. Williams, Impact of the COVID-19 Pandemic Lockdown on Air Pollution in 20 Major Cities around the World. *Atmosphere* **11** (2020).
16. G. I. Gkatzelis *et al.*, The global impacts of COVID-19 lockdowns on urban air pollution. *Elementa: Science of the Anthropocene* **9** (2021).
17. Z. S. Venter, K. Aunan, S. Chowdhury, J. Lelieveld, COVID-19 lockdowns cause global air pollution declines. *Proc Natl Acad Sci U S A* **117**, 18984-18990 (2020).
18. Z. Zhang, A. Arshad, C. Zhang, S. Hussain, W. Li, Unprecedented Temporary Reduction in Global Air Pollution Associated with COVID-19 Forced Confinement: A Continental and City Scale Analysis. *Remote Sensing* **12** (2020).
19. P. Sicard *et al.*, Amplified ozone pollution in cities during the COVID-19 lockdown. *Sci Total Environ* **735**, 139542 (2020).
20. K. B. Kazuyuki Miyazaki1*, 2, Takashi Sekiya3, Masayuki Takigawa3, Jessica L. Neu1, Kengo Sudo3,4, Greg Osterman1, Henk Eskes5, Global tropospheric ozone responses to reduced NOx emissions linked to the COVID-19 worldwide lockdowns. *SCIENCE ADVANCES* **7 : eabf7460 9 June 2021** (2021).
21. Q.-X. Chen, C.-L. Huang, Y. Yuan, H.-P. Tan, Influence of COVID-19 Event on Air Quality and their Association in Mainland China. *Aerosol and Air Quality Research* **20**, 1541-1551 (2020).
22. Y. Zhao *et al.*, Substantial Changes in Nitrogen Dioxide and Ozone after Excluding Meteorological Impacts during the COVID-19 Outbreak in Mainland China. *Environmental Science & Technology Letters* **7**, 402-408 (2020).
23. Y. Wang *et al.*, Changes in air quality related to the control of coronavirus in China: Implications for traffic and industrial emissions. *Sci Total Environ* **731**, 139133 (2020).
24. Y. W. Tianhao Le, Lang Liu, Jiani Yang, Yuk L. Yung, Guohui Li, John H. Seinfeld, Unexpected air pollution with marked emission reductions during the COVID-19 outbreak in China. *Science* **10.1126/science.abb7431** (2020).
25. B. Bekbulat *et al.*, Changes in criteria air pollution levels in the US before, during, and after Covid-19 stay-at-home orders: Evidence from regulatory monitors. *Sci Total Environ* **769**, 144693 (2021).

26. B. Siciliano, G. Dantas, C. M. da Silva, G. Arbilla, Increased ozone levels during the COVID-19 lockdown: Analysis for the city of Rio de Janeiro, Brazil. *Sci Total Environ* **737**, 139765 (2020).

27. Q. Zhang *et al.*, Substantial nitrogen oxides emission reduction from China due to COVID-19 and its impact on surface ozone and aerosol pollution. *Sci Total Environ* **753**, 142238 (2021).

28. Q. Yuan *et al.*, Spatiotemporal variations and reduction of air pollutants during the COVID-19 pandemic in a megacity of Yangtze River Delta in China. *Sci Total Environ* **751**, 141820 (2021).

29. L. Wang *et al.*, Unexpected rise of ozone in urban and rural areas, and sulfur dioxide in rural areas during the coronavirus city lockdown in Hangzhou, China: implications for air quality. *Environ Chem Lett* **18**, 1713-1723 (2020).

30. H. Wang *et al.*, Characterization of the aerosol chemical composition during the COVID-19 lockdown period in Suzhou in the Yangtze River Delta, China. *J Environ Sci (China)* **102**, 110-122 (2021).

31. Y. Lv *et al.*, Meteorology-normalized variations of air quality during the COVID-19 lockdown in three Chinese megacities. *Atmos Pollut Res* **13**, 101452 (2022).

32. X. Lian *et al.*, Impact of city lockdown on the air quality of COVID-19-hit of Wuhan city. *Sci Total Environ* **742**, 140556 (2020).

33. Z. Shi *et al.*, Abrupt but smaller than expected changes in surface air quality attributable to COVID-19 lockdowns. *Sci Adv* **7** (2021).

34. X. Huang *et al.*, Enhanced secondary pollution offset reduction of primary emissions during COVID-19 lockdown in China. *national science review* 10.31223/osf.Io/hvuzy (2020).

35. X. Shi, G. P. Brasseur, The Response in Air Quality to the Reduction of Chinese Economic Activities During the COVID-19 Outbreak. *Geophys Res Lett* **47**, e2020GL088070 (2020).

36. Z. Zhang *et al.*, Attributing Increases in Ozone to Accelerated Oxidation of Volatile Organic Compounds at Reduced Nitrogen Oxides Concentrations. *PNAS Nexus* **1** (2022).

37. Y. Tan, T. Wang, What caused ozone pollution during the 2022 Shanghai lockdown? Insights from ground and satellite observations. *Atmospheric Chemistry and Physics* **22**, 14455-14466 (2022).

38. C.-A. Q. D. Collection, COVID-19 Air Quality Data Collection (2021), version 4, last updated 2022-01-31 from: https://covid-aqs.fz-juelich.de. .

39. K. Xu *et al.*, Air Quality Index, Indicatory Air Pollutants and Impact of COVID-19 Event on the Air Quality near Central China. *Aerosol and Air Quality Research* **20**, 1204-1221 (2020).

40. K. Xu *et al.*, Impact of the COVID-19 Event on Air Quality in Central China. *Aerosol and Air Quality Research* **20**, 915-929 (2020).

41. S. Wan *et al.*, Impact of the COVID-19 Event on Trip Intensity and Air Quality in Southern China. *Aerosol and Air Quality Research* **20**, 1727-1747 (2020).

42. Z. Li *et al.*, Impact of the COVID-19 Event on the Characteristics of Atmospheric Single Particle in the Northern China. *Aerosol and Air Quality Research* **20**, 1716-1726 (2020).
43. H. Patel *et al.*, Implications for air quality management of changes in air quality during lockdown in Auckland (New Zealand) in response to the 2020 SARS-CoV-2 epidemic. *Sci Total Environ* **746**, 141129 (2020).
44. S. Sharma *et al.*, Effect of restricted emissions during COVID-19 on air quality in India. *Sci Total Environ* **728**, 138878 (2020).
45. S. Selvam *et al.*, SARS-CoV-2 pandemic lockdown: Effects on air quality in the industrialized Gujarat state of India. *Sci Total Environ* **737**, 140391 (2020).
46. A. Tobias *et al.*, Changes in air quality during the lockdown in Barcelona (Spain) one month into the SARS-CoV-2 epidemic. *Sci Total Environ* **726**, 138540 (2020).
47. W. P. L. Carter, Development of the SAPRC-07 chemical mechanism. *Atmospheric Environment* **44**, 5324-5335 (2010).
48. E. Nie *et al.*, Emission characteristics of VOCs and potential ozone formation from a full-scale sewage sludge composting plant. *Sci Total Environ* **659**, 664-672 (2019).
49. M. Wang *et al.*, Ozone pollution characteristics and sensitivity analysis using an observation-based model in Nanjing, Yangtze River Delta Region of China. *J Environ Sci (China)* **93**, 13-22 (2020).
50. Z. Li *et al.*, The Modeling Study about Impacts of Emission Control Policies for Chinese 14th Five-Year Plan on PM2.5 and O3 in Yangtze River Delta, China. *Atmosphere* **13** (2021).
51. H. R. Simon, A.; Wells, B.; Xing, J.; Frank, N. , Ozone Trends Across the United States over a Period of Decreasing NOx and VOC Emissions. . *Environ. Sci. Technol.* **49**, 186-195 (2015).
52. Z. Li *et al.*, Oxidizing capacity of the rural atmosphere in Hong Kong, Southern China. *Sci Total Environ* **612**, 1114-1122 (2018).
53. F. Wang *et al.*, Impacts of uncertainty in AVOC emissions on the summer ROx budget and ozone production rate in the three most rapidly-developing economic growth regions of China. *Advances in Atmospheric Sciences* **31**, 1331-1342 (2014).
54. J. Zhu *et al.*, Observationally constrained modeling of atmospheric oxidation capacity and photochemical reactivity in Shanghai, China. *Atmospheric Chemistry and Physics* **20**, 1217-1232 (2020).
55. K. Ropkins, J. E. Tate, Early observations on the impact of the COVID-19 lockdown on air quality trends across the UK. *Sci Total Environ* **754**, 142374 (2021).
56. C. Ordonez, J. M. Garrido-Perez, R. Garcia-Herrera, Early spring near-surface ozone in Europe during the COVID-19 shutdown: Meteorological effects outweigh emission changes. *Sci Total Environ* **747**, 141322 (2020).
57. C. A. Cardelino, W. L. Chameides, An observation-based model for analyzing ozone precursor relationships in the urban atmosphere. *J Air Waste Manag Assoc* **45**, 161-180 (1995).

58. K. W. Appel *et al.*, The Community Multiscale Air Quality (CMAQ) model versions 5.3 and 5.3.1: system updates and evaluation. *Geosci Model Dev* **14**, 2867-2897 (2021).
59. B. N. Murphy *et al.*, The Detailed Emissions Scaling, Isolation, and Diagnostic (DESID) module in the Community Multiscale Air Quality (CMAQ) modeling system version 5.3.2. *Geosci Model Dev* **14**, 3407-3420 (2021).
60. Edgar (2019) joint research centre. emissions database for global atmospheric research.
61. J. An *et al.*, Emission inventory of air pollutants and chemical speciation for specific anthropogenic sources based on local measurements in the Yangtze River Delta region, China. *Atmospheric Chemistry and Physics* **21**, 2003-2025 (2021).
62. X. Chen *et al.*, A high temporal-spatial emission inventory and updated emission factors for coal-fired power plants in Shanghai, China. *Sci Total Environ* **688**, 94-102 (2019).
63. J. Feng *et al.*, Effluent concentration and removal efficiency of nine heavy metals in secondary treatment plants in Shanghai, China. *Environ Sci Pollut Res Int* **25**, 17058-17065 (2018).
64. H. Xu *et al.*, Quantifying aircraft emissions of Shanghai Pudong International Airport with aircraft ground operational data. *Environ Pollut* **261**, 114115 (2020).
65. X. Chen *et al.*, Emission characteristics of fine particulate matter from ultra-low emission power plants. *Environ Pollut* **255**, 113157 (2019).
66. J. Gao *et al.*, A case study of surface ozone source apportionment during a high concentration episode, under frequent shifting wind conditions over the Yangtze River Delta, China. *Science of The Total Environment* **544**, 853-863 (2016).
67. L. Li *et al.*, Source apportionment of fine particles and its chemical components over the Yangtze River Delta, China during a heavy haze pollution episode. *Atmospheric Environment* **123**, 415-429 (2015).
68. R. Dang, H. Liao, Radiative Forcing and Health Impact of Aerosols and Ozone in China as the Consequence of Clean Air Actions over 2012–2017. *Geophysical Research Letters* **46**, 12511-12519 (2019).
69. J. B. Wu *et al.*, Development of an on-line source-tagged model for sulfate, nitrate and ammonium: A modeling study for highly polluted periods in Shanghai, China. *Environ Pollut* **221**, 168-179 (2017).
70. Q. Wang *et al.*, Regional Transport of PM2.5 and O3 Based on Complex Network Method and Chemical Transport Model in the Yangtze River Delta, China. *Journal of Geophysical Research: Atmospheres* **127** (2022).

Figures and Tables

Figure 1. The lockdown period for the six megacities (A). Percentage changes of the six criteria pollutants during CLPs compared to previous years (B). Diurnal variation of the pollutants during the lockdown period for the six megacities (C). The colorful plot shows the diurnal variation of the pollutants during the lockdown period and the gray plot is for the previous years. The continuous line and the dotted line represent the mean and median, respectively, and the shaded region shows the IQR (25^{th} and 75^{th} percentile) of mean diurnal variation observed at the national sites in the respective cities.

Figure 2. Diurnal variation of the pollutants during CLPs for the typical monitoring sites in Shanghai. The colorful plot shows the diurnal variation of the pollutants during CLPs and the gray plot is for the last year. The continuous line and the dotted line represent the mean and median, respectively, and the shaded region shows the IQR.

Figure 3. Contribution ratios of ozone formation potentials of VOC groups in three stations (A). Concentrations of ozone formation potentials of the top 20 VOC components in three stations (B). The outer circle shows the ratios of OFP during CLP-22 and the inner circle shows the same period for the previous year. The outer bar means the contribution ratios of components larger than 1%, the red bar means the concentration of OFP during CLP-22, and the gray bar represents the same period for the previous year.

Figure 4. Relationship between O_3 concentration and relative humidity and temperature during CLP-22 in three stations (A). Isopleth diagrams of modeled ozone formation potentials on VOCs reactivity, the Mixing ratio of NOx during CLP-22, and the same period for the previous year in three stations (B).

Figure 5. Response of O_3 concentration including the average daily maximum O_3 concentration, the average daily MDA8 O_3 concentration, and the average hourly O_3 concentration on different emission control scenarios. The red star means the predicted reduction percentage in three stations according to the observed concentration changes of NO_2 and VOCs.

Figure 6. Contribution of meteorological condition changes and emission changes on the average daily maximum O_3 concentration, the average daily MDA8 O_3 concentration, and the average hourly O_3 concentration.

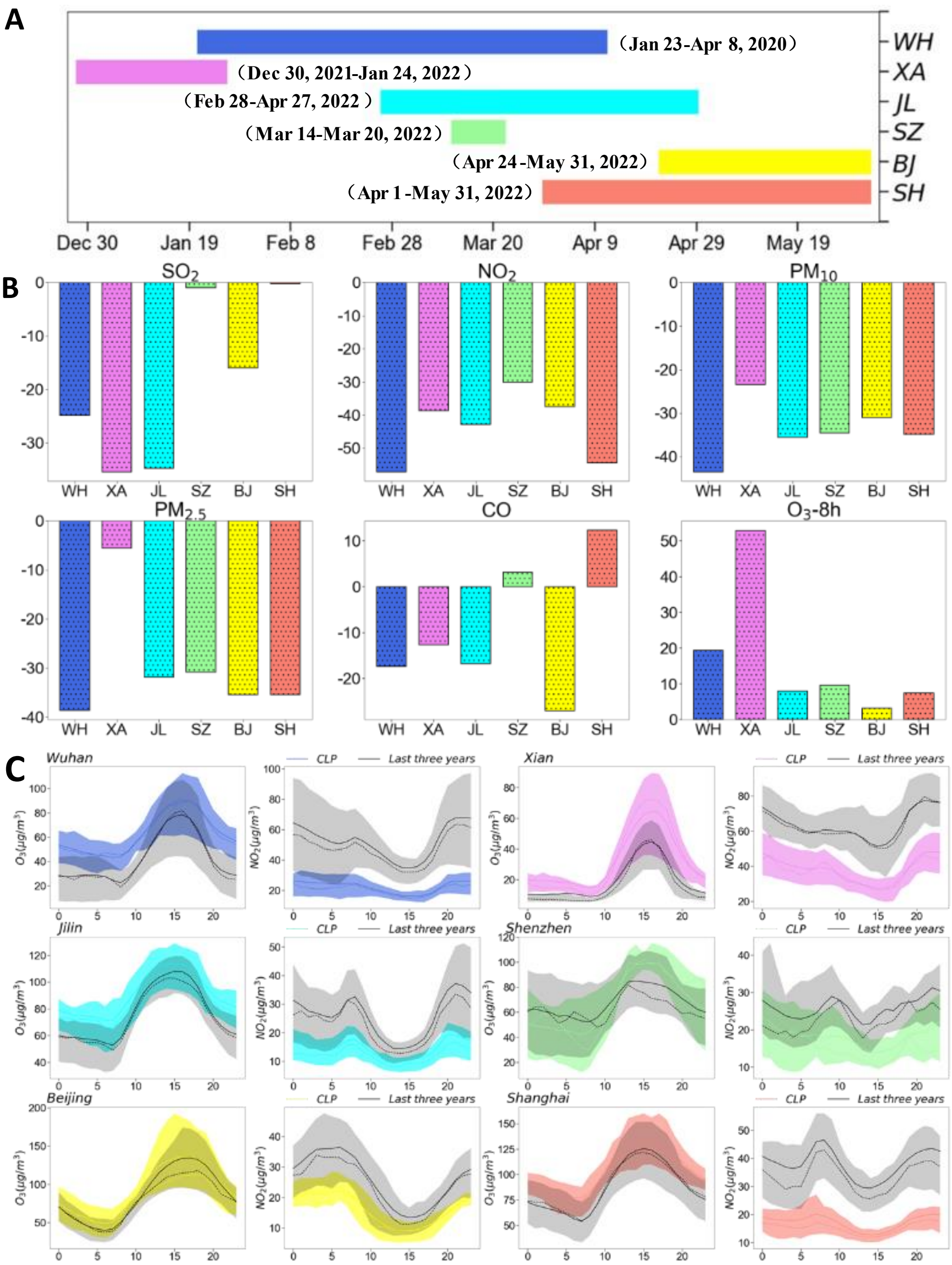

Figure 1. The lockdown period for the six megacities(A). Percentage changes of the six criteria pollutants during CLPs compared to previous years (B). Diurnal variation of the pollutants during the lockdown period for the six megacities (C). The colorful plot shows the diurnal variation of the pollutants during the lockdown period and the gray plot is for the previous years. The continuous line and the dotted line represent the mean and median, respectively, and the shaded region shows the IQR (25th and 75th percentile) of mean diurnal variation observed at the national sites in the respective cities.

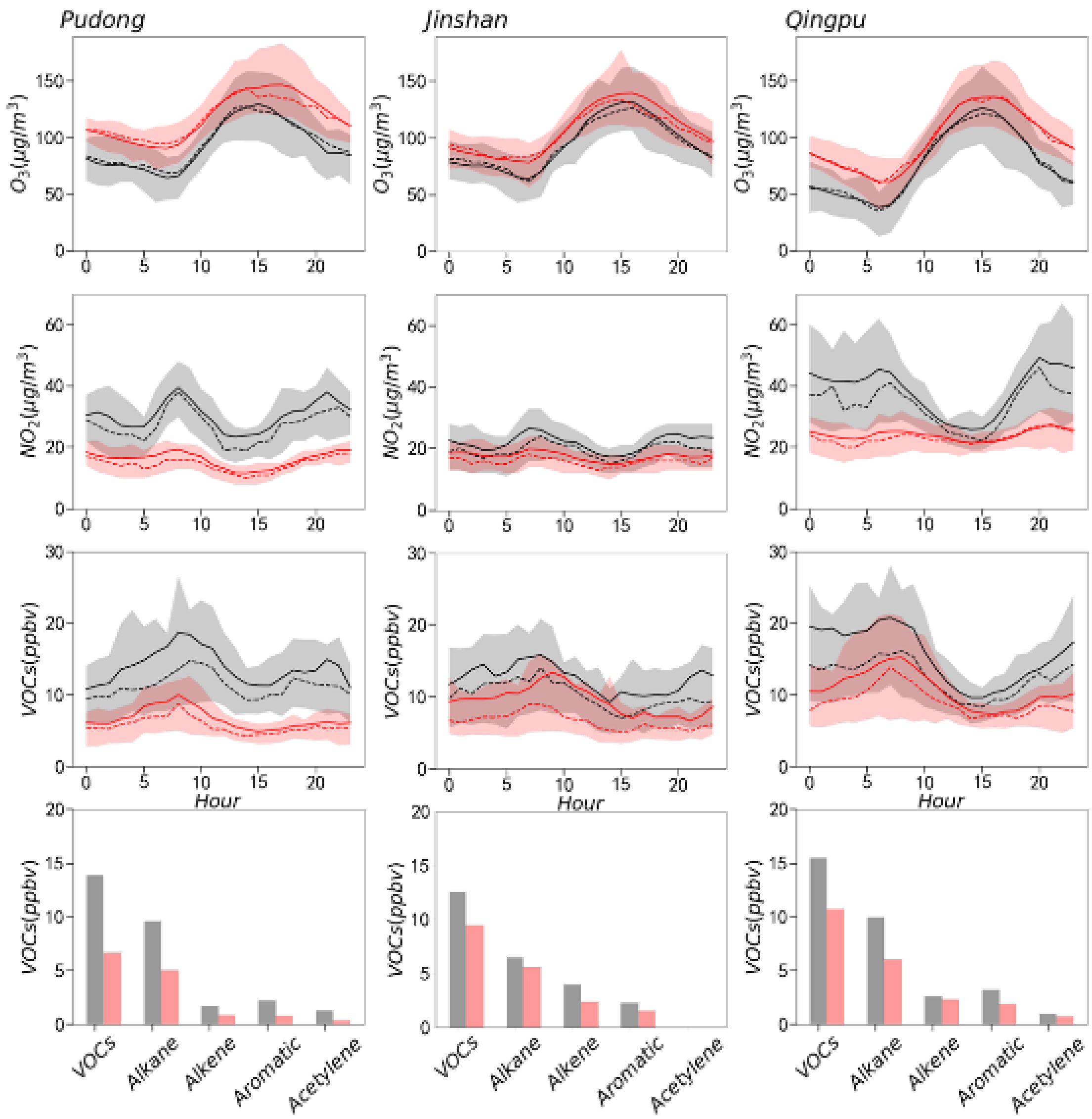

Figure 2. Diurnal variation of the pollutants during CLPs for the typical monitoring sites in Shanghai. The colorful plot shows the diurnal variation of the pollutants during CLPs and the gray plot is for the last year. The continuous line and the dotted line represent the mean and median, respectively, and the shaded region shows the IQR.

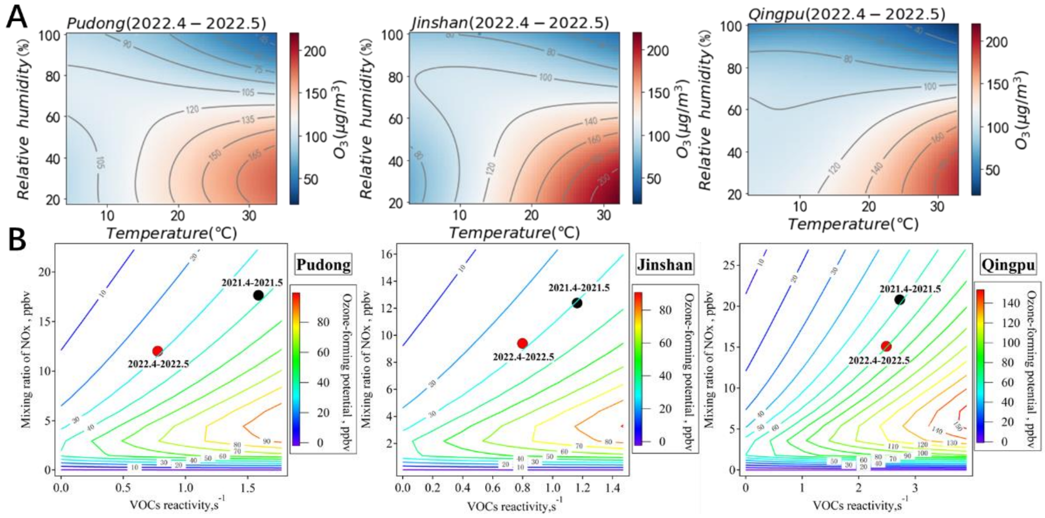

Figure 3. Relationship between O_3 concentration and relative humidity and temperature during CLP-22 in three stations (A). Isopleth diagrams of modeled ozone formation potentials on VOC reactivity, the Mixing ratio of NOx of during CLP-22, and the same period for the previous year in three stations (B).

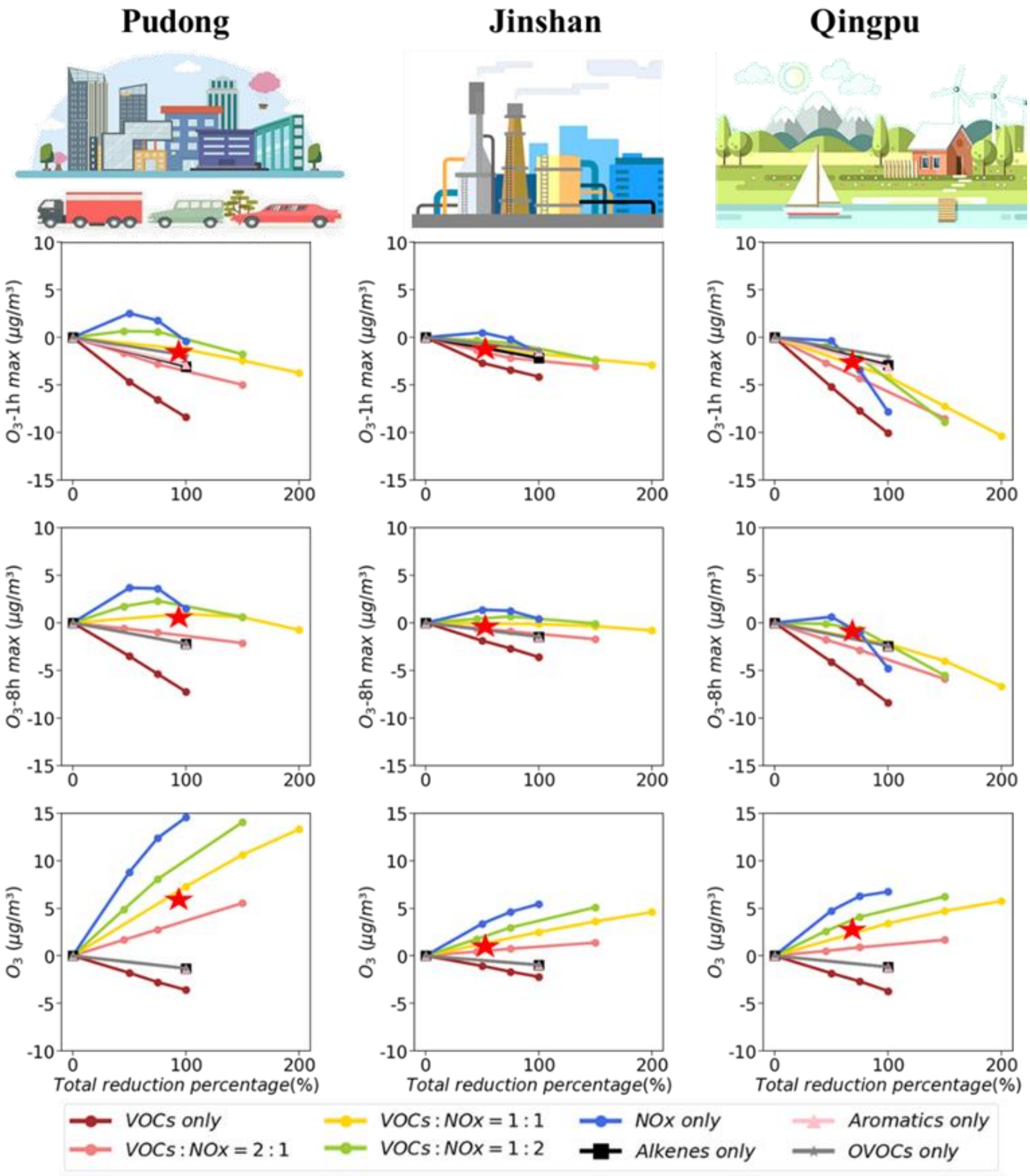

Figure 4. Response of O_3 concentration including the average daily maximum O_3 concentration, the average daily MDA8 O_3 concentration, and the average hourly O_3 concentration on different emission control scenarios. The red star means the predicted reduction percentage in three stations according to the observed concentration changes of NO_2 and VOCs.

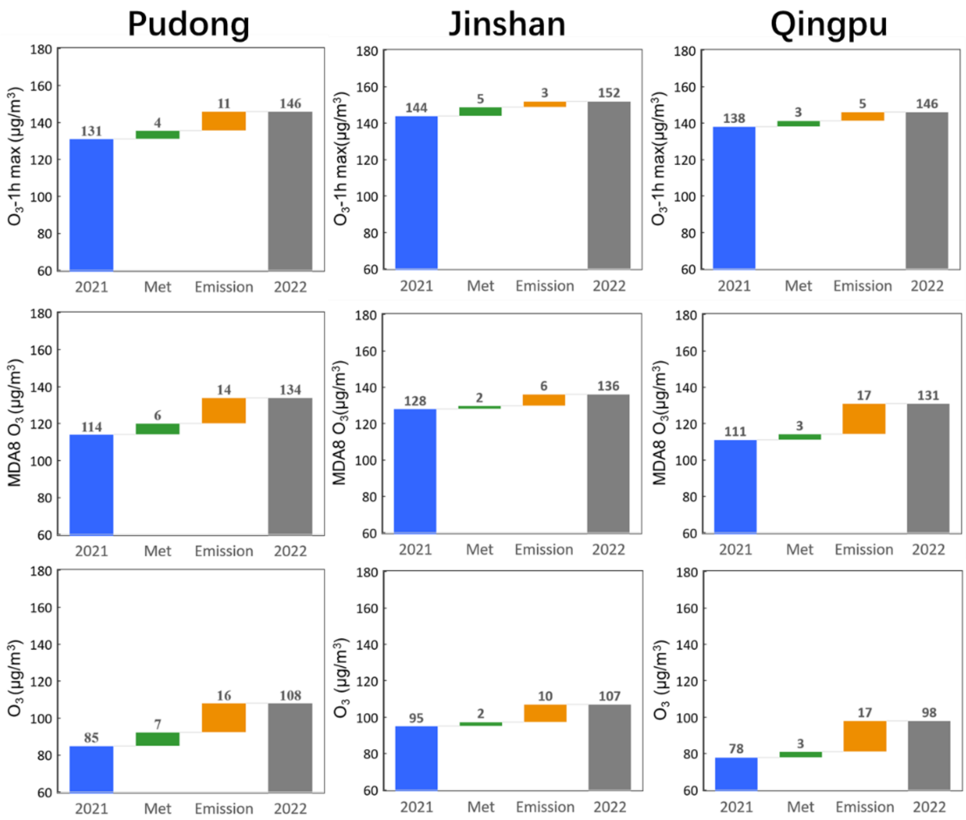

Figure 5. Contribution of meteorological condition changes and emission changes on the average daily maximum O_3 concentration, the average daily MDA8 O_3 concentration, and the average hourly O_3 concentration.